applied optics

Simple telecentric submillimeter lens with near-diffraction-limited performance across an 80 degree field of view

Mohsen Rezaei, Iman Hasani Nia, Alireza Bonakdar, and Hooman Mohseni*

Bio-Inspired Sensors and Optoelectronics Laboratory (BISOL), Department of Electrical Engineering and Computer Science, Northwestern University, Evanston, Illinois 60208, USA
**Corresponding author: hmohseni@northwestern.edu*

Received 13 June 2016; revised 24 September 2016; accepted 27 September 2016; posted 29 September 2016 (Doc. ID 268129); published 26 October 2016

A simple and compact telecentric lens based on two hemispheric optical elements arranged in a formation resembling an "hourglass" is proposed and evaluated. Our modeling and experimental results show the ability of this lens in achieving high resolution over a large field of view. A prototype with 500 μm total thickness is built using silicon micromachining methods for a center wavelength of 1500 nm. Experimental measurement shows near-diffraction-limited performance and good telecentricity over an 80° field of view at a numerical aperture of 0.2. All elements of the hourglass lens are in direct contact, and hence the alignment is extremely simple. We believe the proposed lens is a good candidate for compact and low-cost multi-aperture imagers.

OCIS codes: (110.0110) Imaging systems; (350.3950) Micro-optics; (220.0220) Optical design and fabrication; (220.4000) Microstructure fabrication; (080.3630) Lenses; (220.3620) Lens system design.

http://dx.doi.org/10.1364/AO.55.008752

1. INTRODUCTION

There is a rapidly growing demand for consumer electronic devices with ultracompact form factor and yet massive functionalities. Along with this trend, miniaturized camera modules have found a large number of applications, such as smart phones, webcams, endoscopes, tablets, and portable computers. Design and fabrication of miniature lenses and integration of them with cameras are still the key challenges in making ultrasmall imaging systems. In particular, a tremendous amount of research is ongoing to find low-cost and compact lenses that can produce high-resolution images over a large field of view.

Conventional imaging techniques include sophisticated lens modules with multiple elements to overcome the chromatic dispersion of the materials. A significant amount of research and technology development made it possible to make such compact lenses and integrate them in mobile phones and many electronic devices in subcentimeter dimensions. To reach to a certain resolution for an image sensor, there is a corresponding numerical aperture (NA) that should be considered in the lens design. This will impose a minimum possible thickness for a lens system with a given aperture diameter. The aperture diameter determines the angular resolution of the imaging system [1]. Since there is fundamental limit on the lens thickness for a given aperture size and optical resolution, totally different approach should be exploited to decouple the thickness of the camera module from angular resolution of the imaging system. Multi-aperture imaging is an attractive solution to the form factor problem. It replaces a single aperture with a number of smaller apertures with overlapping fields of view (FOVs) [2]. The small aperture will decrease the focal length, resulting in a thinner camera module. Low angular resolution pictures produced from individual small-aperture imagers are then converted to a high-resolution image, using postprocessing techniques such as super-resolution [3]. Usually, each of these imagers is designed to have a single color to eliminate cross talk between imagers. A full-color, high-resolution image can then be reconstructed using the color information from each aperture. The growing computational powers in the mobile platforms and increased performance of the CMOS imagers have led to the growing popularity of multi-aperture imagers [3–6].

In this paper, we introduce a telecentric lens with near-diffraction-limit resolution across an 80° FOV. In Section 2, we present the lens structure and simulation results using commercial ray tracing software. In Section 3, a method for fabricating a lens holder using micromachining techniques is described. The characterization of the lens in order to extract the point spread function using direct measurement will be described in Section 4. Finally, Section 5 will conclude the paper.

2. PROPOSED LENS STRUCTURE AND SIMULATION RESULTS

In this section, the proposed telecentric lens structure will be discussed. It is composed of two half-ball lenses placed back to back in an hourglass-like configuration (see Fig. 1). In this figure, A and D are the aperture diameter and the half-ball lens diameter, respectively, and G is the gap distance from the back of the lens to the aperture. Since the focal plane of the proposed lens is close to the surface and the aperture is placed in the back focal plane, the lens is telecentric in image space. Telecentricity in image space is an important feature to increase light transmission to the image sensor and to match the NA of the sensor pixels to the NA of the lens across the whole sensor area [7]. Telecentricity is particularly important for large imaging sensors or sensors that have pixel-level functionalities. For example, the extinction ratio of pixel-level polarization imaging sensors can drop by an order of magnitude for incident angles exceeding 18 deg [8].

Special considerations should be made when designing a miniature telecentric lens. Since the aperture should be placed at the back focal plane of the lens to make it telecentric in image space, the minimum thickness from the aperture to the focal plane for a thin lens will be $2f$, where f is the focal length of the lens. The proposed hourglass lens has a total thickness close to the minimum possible limit. As shown in the schematic, the lens configuration has a flat surface, both in the image side and the object side, and there is no gap between the optical elements. This configuration makes it easy to place the lens elements on top of each other and on the surface of the image sensor without the need for accurate spacing. A high-curvature lens surface is one of the key components in making miniature lenses. While spherical aberration is more severe for high-power surfaces, the small size of the lens reduces the aberration. The other important consideration in high-curvature lenses is the antireflection coating of the surface. As we mentioned before, the multi-aperture cameras can be designed to operate such that there is one color per aperture. This approach can dramatically reduce the complexity of the coating, even for a highly curved surface, since each is designed for only a narrow wavelength range.

An hourglass lens structure is modeled using a commercial ray tracing solver (Zemax). General specifications of the lens are listed in Table 1. We used hemispheres with the diameters of 500 μm in our simulations, so the total thickness of the lens is

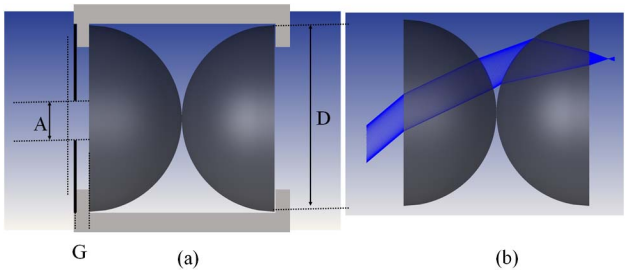

Fig. 1. (a) Schematic diagram for the proposed lens composed of two half-ball lenses placed back to back. D is the diameter of lens, and A is the aperture diameter. (b) Schematic representation for the illumination of the lens.

Table 1. General Lens Specification

Object space NA	0.2
Field of view	80°
Aperture	100 μm
Wavelength	1.55 μm
Image-space telecentric	Yes
Total thickness	<0.6 mm
Material	BK7

smaller than 600 μm. The aperture size is optimized to have the best modulation transfer function (MTF) performance. Our simulations show that increasing aperture size more than 100 μm due to spherical aberration will lead to degradation of the performance of the lens. As shown in Fig. 2, we have MTF > 0.4 at a special frequency of 100 lines/mm across a FOV = 80° for the wavelength of 1550 nm. This special frequency corresponds with 5 μm pixel size for the short-wave infrared (SWIR) camera. BK7 glass is used in all simulations. Simulations show that this lens can be optimized to have near-diffraction-limited performance in visible wavelengths. Due to chromatic aberration, the focus spot will move slightly to a different location for different wavelengths. This make the lens not suitable for high-performance single-lens colored imaging systems before applying some sort of compensation for chromatic aberration.

As we mentioned before, one of the important features of this design is its telecentricity in image space. Figure 3(a) shows the simulation results for the exit angle of the chief ray versus the angle of illumination. It shows that the telecentricity of the lens can be controlled by changing the gap between the backside of the lens and the aperture. Transmission calculations with and without the antireflection (AR) coating are presented in Fig. 3(b). For the coating, we have used the default Zemax quarter-wavelength AR coating. It shows a flat large transmission up to an entrance angle of 30°. The transmission drops by about 10% at the edge of the maximum FOV (i.e., ±40°), with or without the AR coating.

The main step after designing an optical element is tolerance analysis. The goal is to make sure that after assembling the lens system the minimum acceptable performance will be maintained. General tolerances used during this analysis are listed in Table 2. Since there are two hemispheres in our lens system

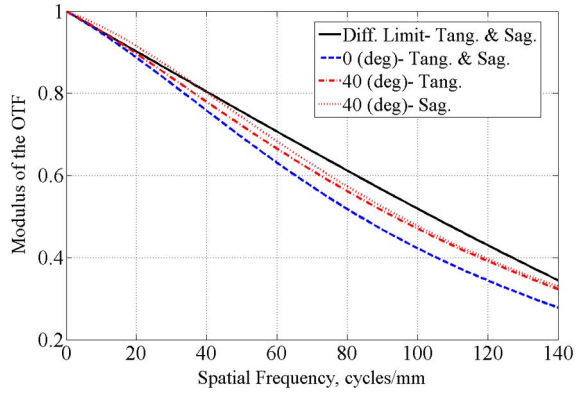

Fig. 2. (a) Modulation transfer function (MTF) for wavelength of 1550 nm.

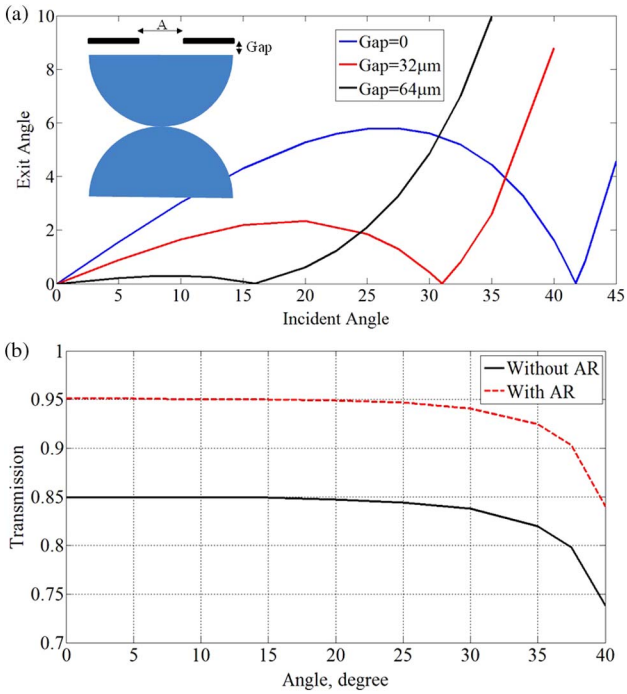

Fig. 3. (a) Telecentricity of the lens for three different gap sizes. (b) Transmission of the lens with AR and without AR coating.

and there is no gap in between them, decentering is the main tolerance factor in assembling. However, with our micromachining method (see Section 3) we are able to achieve centering with an accuracy better than 5 μm. In our analysis, we have assumed 10 μm of tolerance for alignment of the two lenses. Tolerances for the radius of the lens, the refraction index, and the thickness are obtained from manufacturer information.

We have used the automatic procedure of tolerancing by Zemax software. We run a sensitivity analysis for each parameter individually. For criterion of tolerancing, we choose the MTF at a spatial frequency of 100 lines/mm. Any variation from the lens nominal value can slightly change the focal length of the lens. In reality, we can move the lens with respect to the image sensor and adjust for the focal length variation. We consider this readjustment by choosing the compensator to be the back focal distance of the lens. This analysis shows that MTF variation does not exceed 2% for any of tolerances listed above. Finally, the Monte Carlo simulation is employed to consider all the tolerances together. Each parameter is perturbed with Gaussian statistics, and 100 iterations are performed. This analysis indicates that the performance after fabrication will be close to the predicted performance by simulation, with a margin of 5% difference in the MTF.

Table 2. Tolerance Analysis Parameters

Parameter	Tolerance
Decentering	10 μm
Thickness of the half-ball lenses	5%
Refractive index	1%
Radius of curvature	5%

3. MICROMACHINING METHOD FOR FABRICATION OF THE LENS HOLDER

A micromachining process is used to make housing for the lens. For this purpose, a double-sided polished silicon wafer with a thickness of about 550 μm is utilized. Process flow for the fabrication of the microlens holder is shown in Fig. 4. In the first step, a thick layer (12 μm) of the photoresist AZP4620 is spin coated and patterned with the alignment key mask. This patterned PR is used to etch through the wafer in step (b) using a deep reactive ion etcher (STS LpX Pegasus). Etching with this mask and making a hole in the sample will help to align the aperture to the lens opening in step (f). Steps (c) and (d) are for patterning and etching the holder with a 0.5 mm diameter. The etching needs to be stopped at almost 520 μm depth. Deposition of a thick stress-free silicon nitride layer is required to serve as a protection layer. The next two steps of (d) and (e) are used to open the aperture from the back of the wafer. Here, we will use the alignment key to align the aperture with the holder. In the last step, silicon is selectively etched right above the aperture using the KOH solution to form a beveled edge and to increase the FOV. Figure 5 shows the fabricated sample using the developed processing. As this figure shows, arrays of micromachined lenses could be easily fabricated over a large area.

4. LENS CHARACTERISTICS

To measure the 3D point spread function, a customized setup is assembled. As shown in Fig. 6, it consists of three main parts: illumination, a microscope, and an infrared camera. For the illumination, a laser beam at wavelength 1550 nm is collimated and directed using a rotatable mirror to the aperture of the lens

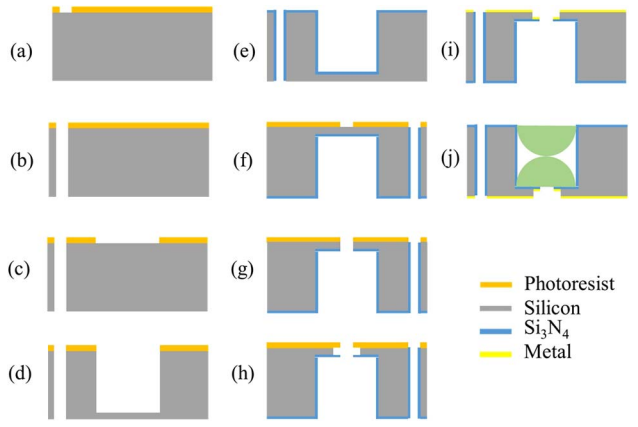

Fig. 4. Process flow to make the holder for the proposed lens. (a) Patterning the alignment key on the photoresist AZP4620. (b) Using the mask to etch from top to the bottom of the sample to have the alignment key on the both sides of the sample. (c) Coating the sample with the photoresist AZP4620 and patterning the lens holder opening. (d) Etching the silicon using the mask. (e) Covering all the surfaces with a silicon nitride-protecting layer. (f) Patterning the aperture at the backside of the sample aligned with the alignment key in step b. (g) Etching the aperture. (h) Using wet etching to open up more to increase the angle of acceptance. (i) Metal evaporation for defining the aperture boundary. (j) Placing the lens inside the holder.

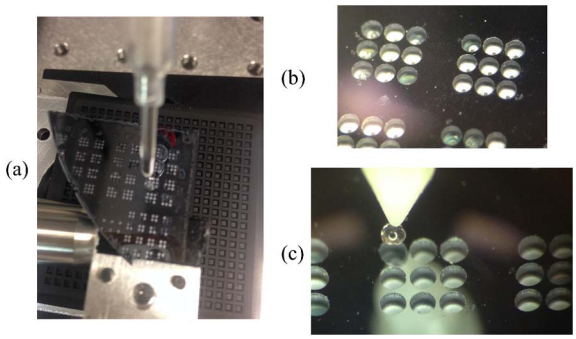

Fig. 5. Microscopic image of the fabricated holder array. (a) Setup to pick up the half-ball lens. (b) Image of the holder arrays. (c) A vacuum tweezer to place the half-ball lens inside the holder.

under test. The beam diameter was large enough to provide the objective lens with an almost uniform illumination over the hourglass lens aperture. An infrared objective lens with a NA of 0.42 is used to capture the light distribution on the other side of the hourglass lens. To image the beam shape and extract the point spread function in 3D, the height of the stage is changed incrementally and image slices of the cross section are acquired by a SWIR camera.

Measurement results for the full width at half-maximum of the beam intensity for different angles of illumination are shown in Fig. 7. To plot this figure for each beam angle, the height of the stage is swiped over 150 μm, with a 5 μm step size. Results show that for the FOV of 80°, we have a flat focal plane with 30 μm depth of focus. Therefore, if the image sensor is placed within this range, the MTF is not affected and 5 μm spot size is maintained. Note that the limited resolution of the objective lens adds a lateral width of about 2.25 μm and an axial width of about 10 μm to this measurement. We also used a conventional microscope to see the image produced by the lens in the visible region (green color) and measure the MTF. An MTF of 0.575 at a spatial frequency of 150 cycles/mm is measured, which is in a very good agreement with the Zemax results for green color. For simplicity, results for the

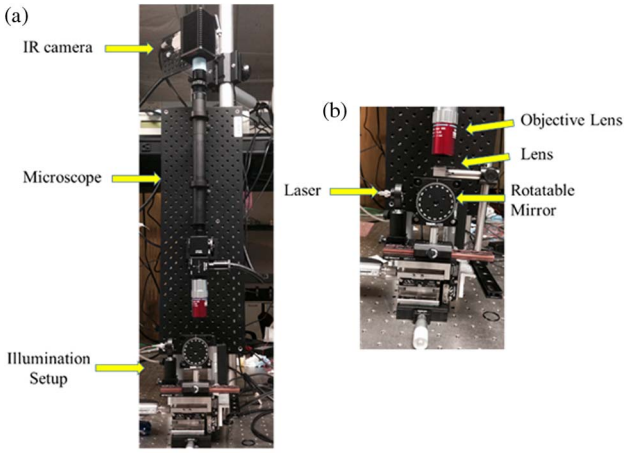

Fig. 6. Characterization setup to image the beam shape and extract the point spread function.

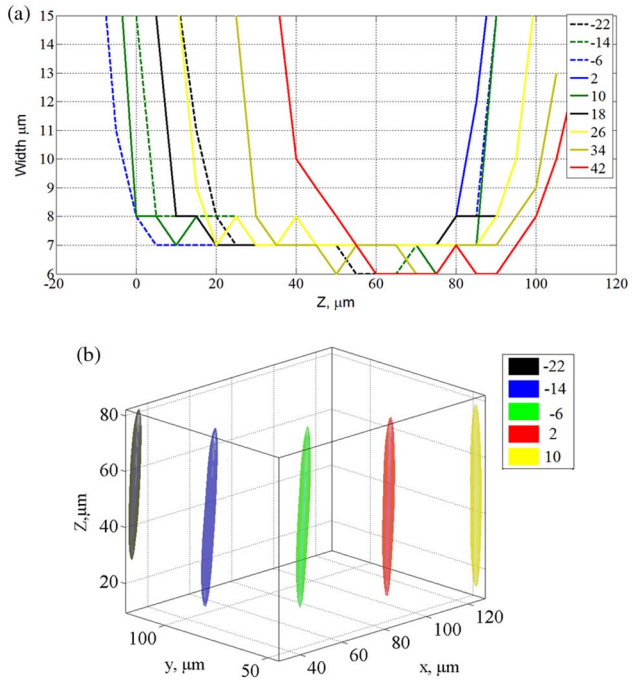

Fig. 7. (a) Measured full width at half-maximum for different angles of incident light. Note that the actual FWHM is about 2.25 μm smaller. (b) Reconstructed 3D view of the focused beam at half of the maximum power for different incident angles.

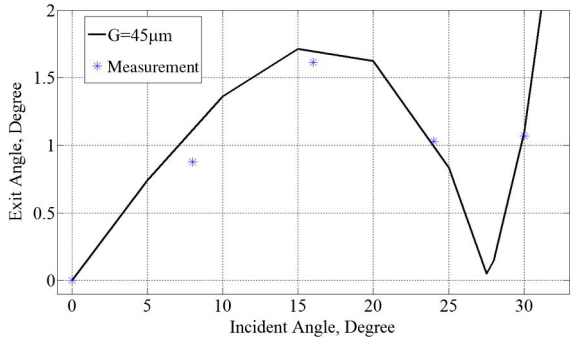

Fig. 8. Measurement and simulation data to show the telecentricity of the lens. The measured exit angles are extracted from Fig. 7(b) and the simulation data are from Fig. 3.

MTF at visible wavelengths are not shown in Fig. 7. Figure 7(b) shows the 3D point spread function for the focused beam. The parallel beams shown in this figure indicate the telecentricity in image space. To quantify the telecentricity of the lens, the exit angles corresponding to each incident angle are extracted from Fig. 7(b). Figure 8 shows the comparison of this measured data with the simulation results shown in Fig. 3. In this plot, for incident angles ranging from 0 to 30 deg, the output angle stays within 2 deg of the lens axis.

5. CONCLUSION

In conclusion, we evaluated and measured the proposed hourglass lens design. It shows high telecentricity in image space,

with a near-diffraction-limit resolution over a large FOV. Its simple design, compactness, and zero spacing between elements make it appealing for miniature cameras. In particular, this lens shows properties suitable for multi-aperture imaging that requires a high FOV, small point spread function, and high telecentricity. Numerical and experimental results show that submillimeter hourglass lenses can perform near ideal spot size and telecentricity. Techniques such as plastic molding or reflow could be used for high-volume manufacturing of these types of lenses.

Funding. National Science Foundation (NSF) (ECCS-0901855, ECCS-1206155, ECCS-1310620); Army Research Office (ARO) (W911NF-11-1-0390, W911NF-13-1-0485).

Acknowledgment. Portions of this work were presented at the SPIE, Current Developments in Lens Design and Optical Engineering in 2015, 957809-1 [9].

REFERENCES

1. J. Tanida, T. Kumagai, K. Yamada, S. Miyatake, K. Ishida, T. Morimoto, N. Kondou, D. Miyazaki, and Y. Ichioka, "Thin observation module by bound optics (tombo): concept and experimental verification," Appl. Opt. **40**, 1806–1813 (2001).
2. K. Venkataraman, D. Lelescu, J. Duparré, A. McMahon, G. Molina, P. Chatterjee, R. Mullis, and S. Nayar, "Picam: an ultra-thin high performance monolithic camera array," ACM Trans. Graph. **32**, 1–13 (2013).
3. A. Portnoy, N. Pitsianis, X. Sun, D. Brady, R. Gibbons, A. Silver, R. T. Kolste, C. Chen, T. Dillon, and D. Prather, "Design and characterization of thin multiple aperture infrared cameras," Appl. Opt. **48**, 2115–2126 (2009).
4. R. Horisaki, K. Kagawa, Y. Nakao, T. Toyoda, Y. Masaki, and J. Tanida, "Irregular lens arrangement design to improve imaging performance of compound-eye imaging systems," Appl. Phys. Express **3**, 022501 (2010).
5. M. Shankar, R. Willett, N. Pitsianis, T. Schulz, R. Gibbons, R. T. Kolste, J. Carriere, C. Chen, D. Prather, and D. Brady, "Thin infrared imaging systems through multichannel sampling," Appl. Opt. **47**, B1–B10 (2008).
6. G. Carles, G. Muyo, N. Bustin, A. Wood, and A. R. Harvey, "Compact multi-aperture imaging with high angular resolution," J. Opt. Soc. Am. A **32**, 411–419 (2015).
7. D. Reshidko and J. Sasian, "Optical analysis of miniature lenses with curved imaging surfaces," Appl. Opt. **54**, E216–E223 (2015).
8. V. Gruev, R. Perkins, and T. York, "CCD polarization imaging sensor with aluminum nanowire optical filters," Opt. Express **18**, 19087–19094 (2010).
9. M. Rezaei, I. Hasani Nia, A. Bonakdar, and H. Mohseni, "Ultra-compact hourglass lens for integrated cameras," Proc. SPIE **9578**, 957809 (2015).